Res Chem Intermed (2009) 35:329–336
DOI 10.1007/s11164-009-0027-7

Preparation of nanocrystalline Fe-doped TiO_2 powders as a visible-light-responsive photocatalyst

Jing Ma · Yi Wei · Wen-Xiu Liu · Wen-Bin Cao

Received: 12 January 2008 / Accepted: 6 June 2008 / Published online: 6 March 2009

Abstract Nanocrystalline Fe-doped TiO_2 powders were prepared using $TiOSO_4$, urea, and $Fe(NO_3)_3 \cdot 9H_2O$ as precursors through a hydrothermal method. The as-synthesized yellowish-colored powders are composed of anatase TiO_2, identified by X-ray diffraction (XRD). The grain size ranged from 9.7 to 12.1 nm, calculated by Scherrer's method. The specific surface area ranged from 141 to 170 m^2/g, obtained by the Brunauer–Emmett–Teller (BET) method. The transmission electron microscopy (TEM) micrograph of the sample shows that the diameter of the grains is uniformly distributed at about 10 nm, which is consistent with that calculated by Scherrer's method. Fe^{3+} and Fe^{2+} have been detected on the surface of TiO_2 powders by X-ray photoelectron spectroscopy (XPS). The UV–Vis diffuse reflection spectra indicate that the light absorption thresholds of the Fe-doped TiO_2 powders have been red-shifted into the visible light region. The photocatalytic activity of the Fe-doped TiO_2 was evaluated through the degradation of methylene blue (MB) under visible light irradiation. The Fe-doped TiO_2 powders have shown good visible-light photocatalytic activities and the maximum degradation ratio is achieved within 4.5 h.

Keywords Fe-doped TiO_2 · Visible light · Hydrothermal method

Introduction

TiO_2 has been extensively researched for the degradation of organic pollutants, for air purification, antibacterial products, as a deodorant, as a demister, etc. [1, 2]. However, the photocatalyst TiO_2 can only be excited by ultraviolet light with a

J. Ma · Y. Wei · W.-X. Liu · W.-B. Cao (✉)
Department of Inorganic Nonmetallic Materials, School of Materials Science and Engineering, University of Science and Technology Beijing, 100083 Beijing, China
e-mail: wbcao@mater.ustb.edu.cn

wavelength less than 387 nm to generate electron–hole pairs due to its wider bandgap of 3.2 eV (anatase). Therefore, it is necessary to improve its visible-light activities by extending its absorption threshold from the UV light region to the visible light region [3, 4]. Doping with Fe ion is one of the best choices to enhance the visible-light photocatalytic activity of TiO_2 [5–8] because the recombination of photogenerated electrons and holes can be hindered by increasing the charge separation. So many works have been done to synthesize Fe-doped TiO_2 powders by a hydrothermal method in recent years [9]. However, the synthesized products need be post-calcinated for the crystallization of TiO_2, which results in the quick grain growth and agglomeration [10].

In this paper, nanocrystalline Fe-doped TiO_2 powders were prepared by a modified hydrothermal method without any post-calcination. The photocatalytic activities of the synthesized Fe-doped TiO_2 powders have been demonstrated by the degradation of methylene blue (MB) aqueous solution under visible-light irradiation.

Experimental

Fe-doped TiO_2 powders have been prepared by a hydrothermal method using $TiOSO_4 \cdot 2H_2O$, urea, distilled water, and $Fe(NO_3)_3 \cdot 9H_2O$ as starting materials. The $TiOSO_4 \cdot 2H_2O$ (0.5 mol) and urea (1 mol) were firstly mixed into distilled water (1 L) and stirred at the speed of 1,000 rpm for 5 min. After that, the $Fe(NO_3)_3 \cdot 9H_2O$ was solved into the suspension based on the desired Fe/Ti ratio: Fe/Ti = 1, 2, 3, 4, 5 at.% (the samples were denoted as FT1, FT2, FT3, FT4, and FT5, respectively). Then, the suspension was stirred for another 10 min. Finally, the obtained suspension was charged into the autoclave with an internal volume of 2 L. The initial pressure was set at 6 MPa and the stirring speed was fixed at about 300 rpm. The autoclave was heated to 150 °C and remained constant for 4 h. The synthesized products were washed by distilled water repeatedly until residual SO_4^{2-} radical could not be detected by 0.5 M $Ba(NO_3)_2$ solution. Finally, the yellowish Fe-doped powders were obtained after vacuum drying at 60 °C for 24 h.

The X-ray diffraction (XRD) measurements were carried out with a diffractometer (type HZG41B-PC) using Cu Kα radiation at a scan rate (2θ) of 0.05°/s to identify the phases composition. The grain size was calculated from the half-height width of different diffraction peaks of the XRD patterns by Scherrer's formula [11]. The lattice constants were calculated by the software package Celerf. X-ray photoelectron spectroscopy (XPS) measurements were performed on a VG Scientific ESCALAB MkII XPS system with a Mg Kα source to analyze the surface elemental composition and valent state of TiO_2. The Brunauer–Emmett–Teller (BET) surface area of the powders was measured by the amount of nitrogen adsorption at 77 K (Quanta chrome, NOVA 1000-TS). A transmission electron microscope (TEM, Hitachi, JEOL-200CX) was used to observe the morphologies of the powders. The UV–Vis diffuse reflection spectra described in this paper were obtained by using a UV–Vis Spectrophotometer (Shimadzu, UV-2100S).

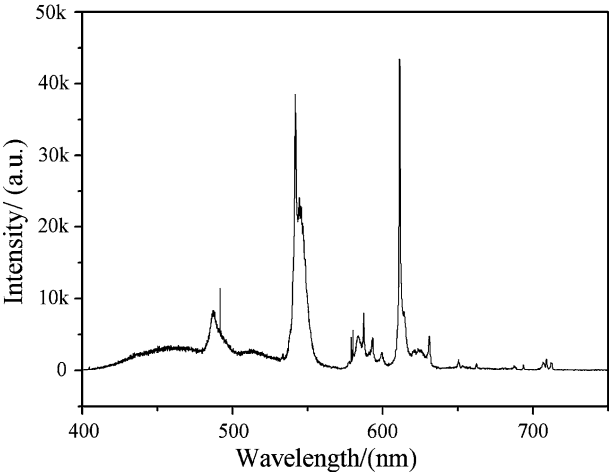

Fig. 1 Fluorescence spectra of the visible-light source

The photocatalytic activities of each sample were tested by the degradation of MB. Four grams of Fe-doped TiO_2 powders were mixed in 400 mL aqueous solution of MB with a concentration of 10 mg/L. The suspensions were stirred by a magnetic stirrer for 2 h in dark to balance the adsorption/desorption of MB. The equilibrium concentration of MB was used as the initial concentration of MB for the photodecomposition processes, and then the suspensions were illuminated with a 23-W lamp, which emits only visible light ranging from 450 to 650 nm, as shown in Fig. 1. Following this, the solutions were irradiated and the specimens of MB suspensions were sampled at intervals of 1.5 h during the degradation process. The TiO_2 powders were separated from the suspensions by using a centrifuge. Then, the concentration of the separated solutions was tested by a TU-1901 UV–Vis spectrophotometer.

Results and discussion

Figure 2 shows the XRD patterns of Fe-doped TiO_2 powders prepared at 150 °C and holding for 4 h. All of the peaks of the XRD patterns in Fig. 2 corresponded to the anatase TiO_2 phase. No peaks of rutile, Fe_2O_3, and $FeTiO_3$ were identified. Table 1 shows the grain size, BET area, crystal constant, and absorption edge of the Fe-doped TiO_2 powders. It can be seen that the grain size of the doped TiO_2 powders were increased from 9.7 to 12.1 nm when the Fe content was increased from 1 to 4 at.%. But the grain size decreased to 10.6 nm when the Fe content was 5 at.%. The specific surface area (SSA) of the powders was firstly decreased from 170 to 141 m^2/g with the increase of Fe content from 1 to 4 at.%, and then the SSA of the powders increased to 156 m^2/g in the case when the Fe content was increased to 5 at.%. Figure 3 shows the TEM micrograph of the sample FT3. The grains were approximatively spherical in shape and the radius of the grains was uniformly

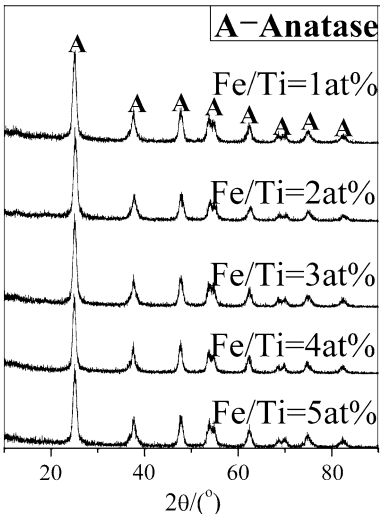

Fig. 2 The X-ray diffraction (XRD) patterns of Fe-doped TiO_2 powders

Table 1 Grain size, Brunauer–Emmett–Teller (BET) area, crystal constant, and absorption edge of Fe-doped TiO_2 powders

Samples	FT1	FT2	FT3	FT4	FT5
Grain size (nm)	9.7	10.6	10.9	12.1	10.6
BET area (m^2/g)	170	160	150	141	156
Crystal constant					
$a = b$ (Å)	3.794	3.801	3.805	3.807	3.797
c (Å)	9.534	9.542	9.534	9.543	9.530
Absorption edge (nm)					
1st	415	435	440	445	446
2nd	540	537	539	541	543

distributed at about 10 nm, which is consistence with the results of Scherrer's method.

Figure 4 shows the XPS spectra of the sample FT3; the Fe 2p region is shown in Fig. 5. It is considered that the binding energy (BE) of Fe^{3+} ions is 711.2 eV and that of Fe^{2+} is 709.3 eV [12]. The Fe 2p peak located at around 710 eV corresponded to the mixtures of Fe_2O_3 and FeO [11], as shown in Fig. 4. This might result from the reduction by the electrons generated by the incident light on the TiO_2 powders. The electron transformation can be illustrated as $Fe^{3+} + e^- \rightarrow Fe^{2+}$.

According to Table 1, the tetragonal lattice parameters determined from the XRD data are slightly larger than those reported from JCPDF data ($a = 3.785$ Å, $c = 9.514$ Å, JCPDF #84-1285). Considering that the ionic radius of octahedrally coordinated Fe^{3+} (0.738 Å) is larger than that of Ti^{4+} (0.610 Å), the increase of the lattice parameter of the as-synthesized samples may suggest that the Fe ion has been incorporated into the anatase lattice and distorted the crystal structure of the host compound.

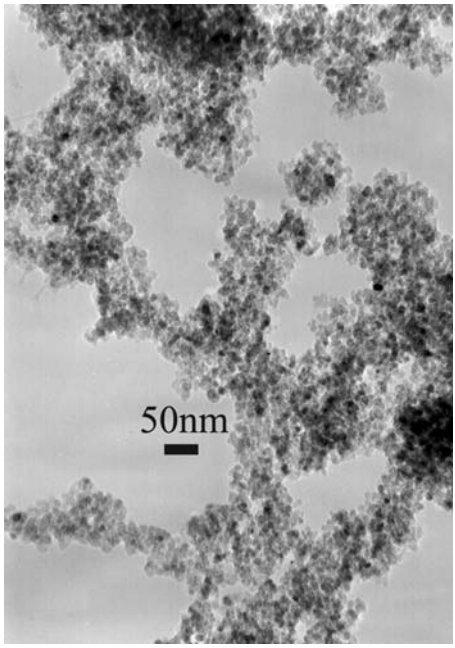

Fig. 3 Transmission electron microscopy (TEM) micrograph of FT3

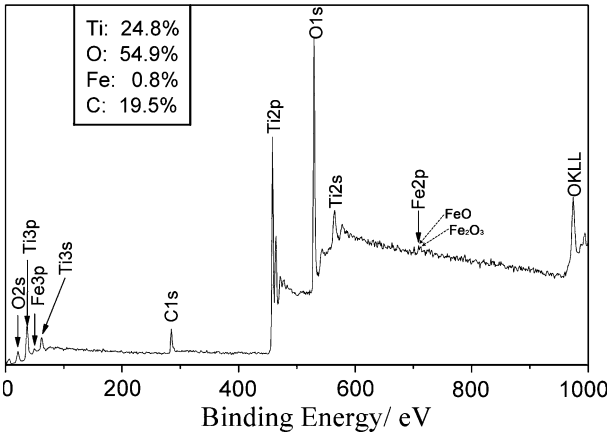

Fig. 4 The Fe 2p peak of FT3

The UV–Vis diffuse reflection spectra of Fe-doped TiO_2 powders are shown in Fig. 5. There are two absorption edges located at 415–450 nm and about 540 nm, respectively. The first absorption threshold located at 415–450 nm was larger than that of non-doped anatase TiO_2. It was thought that some oxygen deficiency in the TiO_2 lattice accounted for the slight red-shift of the absorption thresholds [12]. The second threshold occurring at about 540 nm may be attributed to the doping of

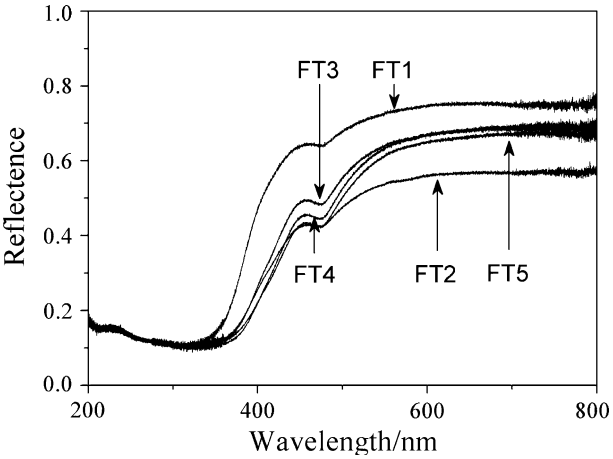

Fig. 5 UV–Vis diffuse reflection spectra of Fe-doped TiO_2 powders

Fe atoms in the lattice of TiO_2. Based on the theory of metal-induced gap states (MIGS), Fe ion doping in the lattice would form an impurity energy level below the conduction band of TiO_2 and, thus, reduce the band-gap energy.

The photocatalytic degradation of the MB solution was investigated by testing the concentrations of MB after the irradiation of visible light at different time intervals. Figure 6 shows the relationship between the degradation time and the concentration of MB during the progress of photocatalytic degradation. According to Fig. 6, the concentration of MB decreased almost linearly and, finally, the MB solution was completely decomposed. After stirring in the dark for 2 h, the concentrations of MB in the suspension with FT1 and FT2 decreased sharply to about 8% of the original concentration, which means that 92% of the MB was

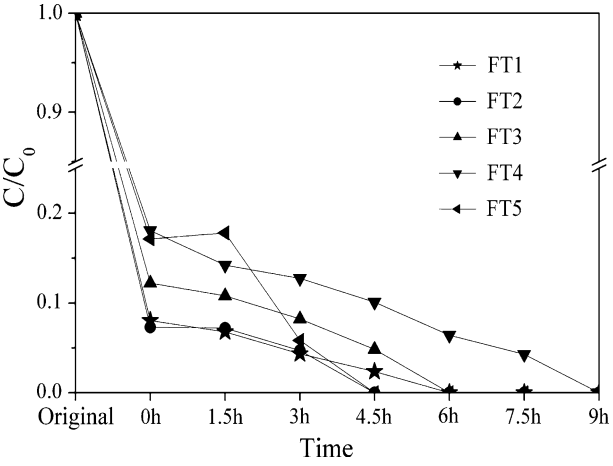

Fig. 6 Photocatalytic degradation of methylene blue (MB) aqueous solution by Fe-doped TiO_2 powders. C_0 = original concentration of MB; C = concentration of MB after photodegradation

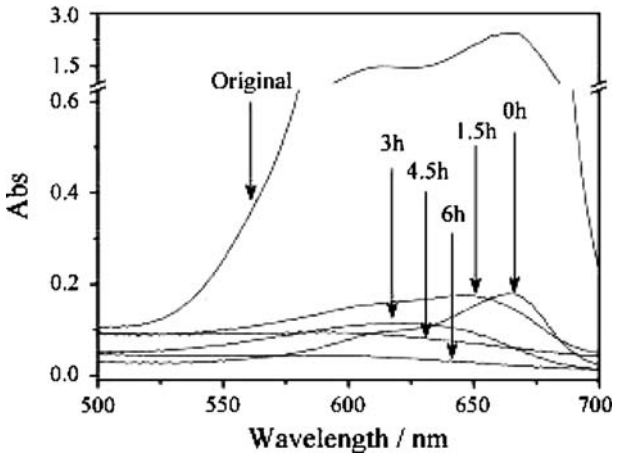

Fig. 7 Absorption spectra of the MB aqueous solution in photocatalytic degradation by FT2

adsorbed on the TiO_2 powders before the start of photocatalytic degradation, whereas about 85, 82, and 83% of the MB was adsorbed by FT3, FT4, and FT5, respectively. The surface of all of the Fe-doped TiO_2 powders was coated in blue as a result of the adsorption of MB. With the progress of photocatalytic degradation, the color of the powders was gradually changed back to be yellowish, which indicates that the adsorbed MB was degraded. Figure 7 shows the absorption spectra of the MB aqueous solution during the process of photodegradation. When the degradation time had elapsed from 0 to 3 h, the absorption peak shifted towards the short-wave direction gradually, which demonstrated that MB had been decomposed into other compounds. After 4.5 h of photodegradation, almost no absorption peak could be detected, which suggested that the MB molecules had finally been decomposed completely. From this point of view, the photocatalytic degradation of MB solution has two steps: adsorption and degradation. At the first stage, the nanocrystalline TiO_2 powders would adsorb the MB molecules due to the higher surface energy, which causes the decrease of the MB concentration before the start of photodegradation; then, the MB will be decomposed gradually after being illuminated with visible-light irradiation.

All of the synthesized Fe-doped TiO_2 powders exhibited good visible-light photocatalytic activities when decomposing MB solution under visible-light irradiation. Zhu et al. [13] reported that the Fe atoms could be incorporated into a lattice of anatase and substitute the Ti atoms with lower Fe concentrations less than 2 wt%, which causes local distortion of the anatase lattice, while some of the Fe atoms will aggregate and form α-Fe_2O_3 when the concentration of Fe was increased to 5 wt%. As XPS data has detected the existence of Fe^{3+} on the surface of the synthesized TiO_2 powders, Fe^{3+} can act as both hole and electron traps to enhance the lifetimes of electrons and holes [14]. If the Fe^{3+} is inserted into the matrix interior of the TiO_2 lattice, the Fe acts as recombination centers for the electron–hole pair [15], as a result of decreased photocatalytic activities. It is

deduced that a certain amount of Fe doping, such as FT2 and FT5, may enhance the photocatalytic activities of TiO_2 powders with different mechanisms.

Conclusions

Visible-light active Fe-doped TiO_2 powders were synthesized through a hydrothermal method by using $TiOSO_4$, H_2O, urea, and $Fe(NO_3)_3 \cdot 9H_2O$ as starting materials. All of the as-synthesized spherical powders are composed of anatase, the grain size ranged from 9.7 to 12.1 nm, and the specific surface area ranged from 141 to 170 m^2/g. The X-ray photoelectron spectroscopy (XPS) data shows that the Fe atoms on the surface of TiO_2 powder exist as both Fe^{3+} and Fe^{2+}. The UV–Vis diffuse reflection spectra of each of the Fe-doped TiO_2 powders have an additional absorption threshold occurring at about 540 nm. The prepared Fe-doped TiO_2 powders have good visible-light response and show good visible-light photocatalytic activities in the degradation of methylene blue (MB). The maximum degradation rate of MB is achieved within 4.5 h of visible-light irradiation by FT2 and FT5.

Acknowledgments The authors appreciate the financial support by the National Natural Science Foundation of China under Grant No. 50772014 and by the Program for New Century Excellent Talents in University under Grant No. NCET-07-0064.

References

1. J.A. Nozik, Annu. Rev. Phys. Chem. **52**, 193–232 (2001)
2. U. Diebold, Surf. Sci. Rep. **48**, 53–229 (2003)
3. D.H. Kim, H.S. Honga, S.J. Kimb et al., J. Alloys Compd. **375**, 259–264 (2004)
4. J.O. Carneiro, V. Teixeiraa, A. Portinhaa et al., Vacuum **78**, 37–46 (2005)
5. W. Zhang, Y. Li, S.L. Zhu et al., Chem. Phys. Lett. **373**, 333–337 (2003)
6. W.Y. Choi, A. Termin, M.R. Hoffmann, J. Phys. Chem. **98**, 13669–13679 (1994)
7. S. Karvinen, P. Hirva, T.A. Pakkanen, J. Mol. Struct.—THEOCHEM **626**, 271 (2003)
8. C.H. Chen, E.M. Kelder, J. Schoonman, Thin Solid Films **342**, 35–41 (1999)
9. J.F. Zhu, Z.G. Deng, F. Chen et al., J. Mol. Catal. A **216**, 35–43 (2004)
10. T. Tong, J. Zhang, F. Chen et al., J. Hazard. Mater. **155**, 572–579 (2008)
11. J.B. Lambert, L. Xue, J.M. Winter, Archaeometry **32**, 47 (1990)
12. I. Justicia, G. Garcia, L. Vazquez et al., Sens. Actuators B **109**, 52–56 (2005)
13. S. Zhu, T. Shi, W. Liu et al., Physica B **396**, 177–180 (2007)
14. J. Zhu, W. Zheng, B. He et al., J. Mol. Catal. A **216**, 35–43 (2004)
15. Z. Li, W. Shen, W. He et al., J. Hazard. Mater. **155**, 590–594 (2008)